Grassi, D., et al. (2017), *Analysis of IR-bright regions of Jupiter in JIRAM-Juno data: Methods and validation of algorithms*, Journal of Quantitative Spectroscopy and Radiative Transfer, 202, doi: 10.1016/j.jqsrt.2017.08.008

accettato per la pubblicazione il 9 agosto 2017.

Analysis of IR-bright regions of Jupiter in JIRAM-Juno data: methods and validation of algorithms

D. Grassi[1,*], N.I. Ignatiev[2], G. Sindoni[1], E. d'Aversa[1], T. Maestri[3], A. Adriani[1], A. Mura[1], G. Filacchione[1], B.M. Dinelli[4], R. Noschese[1], A. Cicchetti[1], G.Piccioni[1], D. Turrini[1,5], F. Tosi[1],M.L. Moriconi[6], A. Olivieri[7], C. Plainaki[8], M. Amoroso[7], S.K. Atreya[9], G.S. Orton[10], S. Bolton[11]

1. Istituto di Astrofisica e Planetologia Spaziali – Istituto Nazionale di Astrofisica, Rome, Italy

2. Institute of Cosmic Research, Russian Academy of Sciences, Moscow, Russia

3. Dipartimento di Fisica e Astronomia, Univ. of Bologna, Italy

4. Istituto di Scienze Atmosferiche e del Clima, Consiglio Nazionale delle Ricerche, Sede di Bologna, Italy

5. Departamento de Fisica, Universidad de Atacama, Copiapò, Chile

6. Istituto di Scienze Atmosferiche e del Clima, Consiglio Nazionale delle Ricerche, Sede di Roma, Italy

7. Agenzia Spaziale Italiana, Sede di Matera, Italy

8. Agenzia Spaziale Italiana, Sede di Roma, Italy

9. Department of Climate and Space Sciences and Engineering, Univ. of Michigan, Ann Arbor, Michigan USA

10. Jet Propulsion Laboratory, California Institute of Technology, Pasadena, California, USA

11. Southwest Research Institute, San Antonio, Texas, USA

* Corresponding author: davide.grassi@iaps.inaf.it

Abstract

In this paper, we detail the retrieval methods developed for the analysis of the spectral data from the JIRAM experiment on board of the Juno NASA mission [1], operating in orbit around Jupiter since July 2016. Our focus is on the analysis of the thermal radiation in the 5 μm transparency window in regions of lesser cloud opacity (namely, hot-spots).

Moving from the preliminary analysis presented in [2], a retrieval scheme has been developed and implemented as a complete end-to-end processing software. Performances in terms of fit quality and retrieval errors are discussed from tests on simulated spectra, while some example and issue from usage on actual Jupiter data are also discussed.

Following the suggestion originally presented in [3] for the analysis of the NIMS data, the state vector to be retrieved has been drastically simplified on physically sounding basis, aiming mostly to distinguish between the 'deep' content of minor gaseous component (water, ammonia, phosphine) and their relative humidity or fractional scale height in the upper troposphere. The retrieval code is based on a Bayesian scheme [4], complemented by simulated annealing method for most problematic cases.

The key parameters retrievable from JIRAM individual spectra are the ammonia and phosphine deep content, the water vapour relative humidity as well as the total aerosol opacity.

Limitations related to the approximations of forward model methods are also assessed quantitatively.

1. Introduction

The Jupiter InfraRed Auroral Mapper (JIRAM) is an instrument on board of the NASA Juno spacecraft [4, 5]. JIRAM includes a slit spectro-imager, operating in the near infrared spectral region (2 - 5 μm) and two image channels. The M filter channel acquires images in a broad spectral range centered around 5 μm, while the L Channel passband is centered around 3.3 μm. The M and L channels are intended to provide the spatial context of the spectral data during the observations of the thermal emissions from the upper troposphere and the aurorae respectively. [1] discussed extensively the science objectives of the JIRAM experiment. Among them, the study of the composition of the upper troposphere and of the properties of the auroral emissions are the ones that have driven both the design of the instrument and the observations planning.

This work describes the main properties and performances of a retrieval code developed for the analysis of JIRAM spectra in the 5 μm methane transparency window to obtain information on the composition of the upper troposphere. In fact, this spectral region is particularly interesting because it hosts the spectral lines of several minor constituents of Jupiter atmosphere like H_2O and NH_3 , that are the main carriers of oxygen and nitrogen in Jupiter atmosphere. Moreover, the 5 μm region is spectrally far enough from the peak of the solar emission and therefore it is largely dominated by the thermal emission of the atmosphere. Figure 1 shows an example of the JIRAM spectrum acquired over an Hot Spot in this spectral region (spectra acquired in daytime conditions also show signal peaks at 2, 2.75 and 2.5 μm due to scattering of solar radiation by residual clouds)

Jupiter emission at 5 μm has been observed at low and intermediate latitudes with space- and ground-based observations (see [6], for a recent example). Few bright distinctive areas were noted: the Hot Spots (the brightest features), associated with the grey 'festoons' observed in the optical domain between the Equatorial zone and the North equatorial Belt; the rim of the Great Red Spot; the entire South Equatorial Zone and the areas surrounding the white ovals in the South-South Tropical Belt. In the bright areas, the thermal photons emitted at an effective level of few bars are marginally absorbed by the clouds, allowing to probe the deeper parts of the troposphere. The ultimate source of opacity at 5 μm is represented by the molecular hydrogen collision-induced absorption, which - even in the absence of other minor components or clouds – reaches an optical thickness of 1 around the 5.5 bars level.

Nonetheless, most of the Jupiter's disk appears dark at 5 μm, suggesting a full coverage by thick clouds: indeed thermochemical equilibrium models for globally averaged conditions of Jupiter [7,8] predict three cloud levels of different compositions - extended over several tens of kilometers in altitude – derived from the condensation of water, ammonia and ammonium hydrosulfide. The brightness temperature study by [9] demonstrated that, at least in the equatorial region, the uppermost level of putative NH_3 ice must have some residual transparency, allowing some radiation from the warmer regions below to escape to space. Further analysis by [10] found that brightness changes at 5 μm are mostly correlated with opacity changes of cloud layers lying at pressure levels between 1 and 2 bars than to variability of the higher ammonia clouds. In accordance with models, these layers are expected to be composed mostly by ammonium hydrosulfide, but the lack of detection of expected spectroscopic signature suggest that a substantial fraction of other materials must also be present.

2. JIRAM data

The JIRAM spectrometer covers the 2-5 μm range with a sampling step of about 10 nm and a nominal t spectral resolution of about 12 nm. The JIRAM spectra are acquired simultaneously along a slit of 256 spatially-adjacent pixels. The field of view of individual pixels (in the spectrometer as well as in the imager) is 250 μrad.

Spatial resolution at the nominal 1-bar level varies greatly because of the large eccentricity of Juno's orbit. Typical science data have resolutions of few hundreds of kilometers.

Juno is a spinning spacecraft, and by design, JIRAM slit is parallel to the spin axis in order to allow rotation compensation during the exposure with typical duration of 1 sec for the spectrometer.

Data acquired during the flyby of the Moon in October 2013 [5] and during the first perijove [11] demonstrated that JIRAM spectrometer benefits from excellent radiometric performances. A preliminary estimate performed prior to Jupiter orbit insertion set the Noise Equivalent Radiance (NER) value at 5 μm around $1.8x10^{-1}$ μW/(cm^2 sr μm). This value was adopted in the analysis described below.

3. Description of the retrieval code

The information content of individual JIRAM spectra has been described in the preparatory work of [2]. Starting from these concepts, we developed an end-to-end retrieval code based on the Bayesian formalism [4]. The code is largely derived from similar software previously developed for the analysis of VIRTIS-Venus Express data [12]. The code is intended to study the composition of the upper troposphere – between the 6 and 1 bar levels – at locations where a moderate cloud optical thickness ($\tau<2$) allows the thermal radiation to be emitted in the considered pressure range for measurements from space. Hot Spots were considered as study cases during development.

The current version of the code (February 2017) includes a forward radiative transfer model based on the correlated-k method [13] considering 30 quadrature points. Multiple scattering by clouds is taken into account through a simple two-streams approach [14]. The retrieval code considers the spectral range between 4 and 5 μm and only the thermal source. While of obvious interest, the inclusion of the solar-dominated spectral range of 2-4 μm would require the treatment of solar scattering, with significant computational burden and considerable uncertainties in the forward modelling errors related to the assumptions on the cloud properties (this is especially true for the upper cloud deck and haze). On the other hand, the 'no solar source' approximation is partly justified by our specific focus on the more transparent regions, assumed to correspond to the brightest areas where the analysis of Drossart et al. [1998], found that the scattered solar contribution is between 100 and 800 times smaller than the thermal component.

The atmosphere is modelled as a stack of 43 plane-parallel levels, uniformly spaced in log(p) between 22 bar and 38 millibar. The vertical temperature profile is fixed and assumed to be the one measured by the Galileo Entry Probe [15].

The code takes into account the opacities of CH_4, H_2O, NH_3, PH_3, AsH_3, GeH_4 and H_2 absorption induced by collisions (CIA) with H_2 itself, He and CH_4. The treatment of the far wing shapes and line cut-offs values as long as the spectroscopic data for these gases are similar to those reported in [2]. A few differences should be noted: data derived from HITRAN were updated to the latest HITRAN 2012 release [16], the line-mixing effects for the strongest lines of ν_3 CH_4 band were included according to the method described in [17], phosphine line parameters were integrated with the publicly-available section of the data described in [18,19].

Following [20], we adopted a very simple model for the putative NH_4SH cloud, assumed to have a single scattering albedo $\omega=0.9$ and an Henyey-Greenstein phase function derived using an asymmetry factor $g=0.7$ in the entire spectral range of interest. This cloud is assumed to lie at the 1 bar level, a value roughly consistent with the GEP nephelometer data [21]. This is the only cloud included in our retrieval scheme. This assumption is indeed rather strong, since it has been derived from the very specific conditions (extreme dryness, very low opacity) experienced by the GEP. In matter of fact, care shall be exercised in interpreting results for opacities at 5 μm greater than an approximative value of 2, since these could likely correspond to more complex cloud structures. Namely, with increasing optical thickness, clouds are expected to become more extended in altitude (with a non negligible gradient of opacity along air temperature) and to show considerable opacities well below the 2 bar level [8].

Following the approach presented in [3], we considered a rather simple set of free atmospheric parameters to model the observed spectra. The vertical mixing ratios of H_2O and NH_3 are described by two free parameters each: an altitude-independent relative humidity, for altitudes above the condensation level and a uniform deep mixing ratio for altitudes below the condensation level. PH_3 vertical mixing ratio is considered to be uniform below the 1 bar level, while above this level it decreases with increasing altitude according to a fixed relative fraction of the local scale height. AsH_3 and GeH_4 mixing ratios are allowed to vary, but are assumed to be uniform with altitude. The last free parameter is the total opacity of the 1-bar cloud. Figure 2 summarizes the free parameters of the retrieval code.

The retrieval of the above mentioned parameters is performed using an iterative Gauss-Newton procedure, inclusive of a Levenberg-Marquardt method ([4], eq. 5.36), required to avoid convergence to local minima. The iterations stop when the changes of the retrieved parameters between consecutive iterations are within the formal retrieval errors. More precisely, we adopted the d_i^2 criterion given by expression (5.29) in [4]. A final evaluation is performed comparing the residuals and JIRAM NER: a simulated annealing method (as presented by [22]) is eventually invoked if the value of χ^2 (defined for this purpose as the mean quadratic difference between the best-fit and observed spectrum as weighted by the NER) exceeds a given threshold level.

We choose to retrieve the logarithm of the free parameters (i.e.: the elements of the state vector) to avoid non-physical negative values. The a priori values of the state vector, as well as the corresponding standard deviations used to build up the uncorrelated a priori covariance matrix S_a are taken from [3] and are listed in Table I. Note that the tests described in section 4 demonstrated the actual insensitivity of our data to the ammonia relative humidity and phosphine scale height: consistently, these parameters are not reported in Table I. Off-diagonal elements of S_a are set to zero.

	$[H_2O]_{deep}$	$[H_2O]_{RH}$	$[NH_3]_{deep}$	$[PH_3]_{deep}$	$[AsH_3]_{deep}$	$[GeH_4]_{deep}$	τ @ 5μ
A priori							
x_a	-2.74	1.00	-3.66	-6.22	-9.34	-9.62	0.
10^{xa}	$1.81 \cdot 10^{-3}$ [ppv]	10. [%]	$2.2 \cdot 10^{-4}$ [ppv]	$6. \cdot 10^{-7}$ [ppv]	$4.5 \cdot 10^{-10}$ [ppv]	$2.4 \cdot 10^{-10}$ [ppv]	1.
$\sigma(x_a)$	1.0	0.48	0.56	0.63	0.5	0.5	1.
$\sigma(x)$	0.884	0.012	0.012	0.006	-	-	0.005

Table I. Retrieved parameters: x_a is the a priori value of the parameter, while the 10^{xa} elements give the equivalent, commonly-used, physical quantities (ppv stands for parts per volume, i.e. molar fraction). $\sigma(x_a)$ is the corresponding standard deviation used to build the S_a covariance matrix, and $\sigma(x)$ is the square root of the covariance matrix S of the retrieval, as computed at the first iteration.

4. Validation

Our analysis tools have been preliminary validated on simulated observations, prior to the orbit insertion of Juno. These activities, described in this section 4, were performed by removing from atmospheric composition germane, arsine and carbon monoxide, whose spectral effects, were deemed as minor compared to the to spectral signatures of methane, water, ammonia and phosphine, as discussed in [2].

4.1 Forward model approximations

The errors introduced by the approximations made in the development of the forward model have been estimated statistically with numerical tests. First, we created a population of different input state vectors. Then, for each state vector, we computed the simulated spectrum with a) the algorithm embedded in the retrieval code b) with a *much* slower full physic line-by-line code. In the latter case we used a much finer vertical discretization (171 levels) and the scattering was accounted for with the DISORT algorithm [23], after the expansion of the Heyney-Greenstein phase function (with g=0.7) in Legendre polynomials. Statistical comparison of spectra a) against their b) counterparts allows a quantitative assessment of the impact of the forward model approximations. The population of the input state vectors was created as follows. For each element of the population:

1. We created a set of 7 (statistically independent) random numbers with zero mean and standard deviation of 1
2. The $\sigma(x_a)$ was multiplied by these random numbers and added to the x_a elements listed in Table I. This returned a random state vector (note that, albeit not reported in Table I, ammonia relative humidity and phosphine scale height were included as free parameters in this test)

The test was repeated for 256 cases (total size of the test population), the size being justified by the aim to reproduce a JIRAM slit. Noteworthy, while the different elements of the input state vector for each case are statistically independent, this is not the case for the corresponding elements of different cases. A correlation length of 35 pixel was imposed, with the purpose to simulate extended spatial features as seen over the Jupiter disk.

Since we are interested mostly in the IR bright areas, the spectra comparison was limited to cases where the residual opacity of the 1-bar cloud was less than 1: this reduced the effective population size to 143. Figures 3a and 3b show the results in relative as well as absolute terms. Albeit the performance of the forward model are – at least in the spectral regions with high signal - in line with those expected for the correlated-k methods (better than 5% for the NEMESIS code [13]), they remain inadequate to fully exploit the excellent radiometric performances of JIRAM. At worse, the ratio between random modeling error and NER reaches values up to 15. Further tests – performed introducing the modeling approximations one by one and considering the mean amplitude of induced errors - demonstrated that the random modeling errors are mostly caused by the treatment of the scattering (consistently, they tend to diminish with decreasing residual opacity), secondly to the usage of correlated-k method instead of a full line-by-line approach and only marginally to coarser vertical sampling grid. The order is reversed for the systematic components. Despite the obvious limitations described above, no viable alternative is presently available for the forward modeling, since both the usage of DISORT or the adoption of a line-by-line code would increase the retrieval time from few minutes to few hours. Net effects of this compromise are described in the following section.

4.2 Retrieval performances

Validation of the retrieval code consists essentially in a direct estimate of the retrieval errors from numerical tests. Errors may arise from several factors:

1. Discrepancies between observed and best-fit spectrum. In the ideal case, this difference would show random fluctuations with a standard deviation equal to NER.
2. Approximations in the forward radiative transfer model, computing time driven (namely: correlated-k instead of line-by-line and two-streams instead of DISORT).
3. Uncertainties in the adopted parameterization of the vertical distribution of the gases.
4. Uncertainties in the spectroscopic aerosol and gas models (aerosol phase functions, spectroscopic line databases, far wing shapes, etc.).

The Bayesan approach directly maps the NER into the retrieval error, therefore point 1 of the above list is formally accounted for (see formula 5.13 in [4]). However, even in the ideal case, significant departures from ideal performances can be induced by the highly non-linear nature of the problem. In order to evaluate these effects, we performed a set of simulated retrievals. We considered the set of simulated observations performed with the forward model embedded in the retrieval code, with the parameters described in section 4.1. We added a random error, with statistical properties equal to JIRAM NER, to the simulated spectrum. Then the simulated noisy spectrum was fed into the retrieval code and the results were compared with the state vector used into the simulation.

Figure 4 shows the results limited to the cases where the residual cloud opacity is smaller than 1. Figure 5 summarizes the modelling capabilities.

The retrieval code has demonstrated to behave nearly ideally: the final χ^2 approaches 1 and the mean values of retrieval errors are close to the square root of the diagonal elements of the covariance matrix of the solution, as listed in the last column of Table I. The relative humidity of ammonia and phosphine scale height were essentially not constrained, demonstrating the effective lack of information content in JIRAM data on these two parameters. This is not surprising, since both parameters describe the vertical profile of these gases at pressure levels not probed by JIRAM weighting functions (as shown in fig.2 of [2]). Deep mixing ratio of water is an ambiguous free parameter: given our parametrization of $[H_2O]$ vs. altitude, only *low* values of $[H_2O]_{deep}$ (approximatively $5 \cdot 10^{-4}$ ppv) determine a condensation level high enough in altitude to place the region of constant mixing ration within the pressure range probed by JIRAM. Conversely, in our simplified model, a constant deep mixing ratio of water is usually achieved well below the region probed by JIRAM weighting functions.

In order to assess the effects of the forward model approximations on the retrievals the same test was repeated analyzing the spectra simulated with the full physic code (line-by-line, DISORT, 171 levels). Figures 6 and 7 summarize the retrieval performances. Noteworthy, the retrieval code is capable to model the observed spectra with an accuracy better than the typical errors associated to the forward model approximations (compare fig. 3a and 7b): some systematic retrieval errors due to over-fit (i.e.: the effort of the algorithm to match the data at the level of formal NER despite actual greater forward modeling uncertainities) of data are therefore to be expected. Albeit the radiative transfer approximations reduce the overall performances, the code retains its capability to reduce substantially the uncertainty with respect to the realistic variations used to define the a priori variance. Table II summarizes retrieval performances as inferred from these two numerical tests. The parameter most adversely affected by forward model approximations is probably the total opacity: the slight systematic excess in the estimate of radiance for a given state vector are erroneously compensated during the retrieval increasing the retrieved values of the opacity. This effect is particularly evident for very low opacity values.

The same numerical approach is less effective for factors 3 and 4. Here, we are not dealing with deliberate simplifications, but with alternative hypothesis to our best-guess assumptions. Therefore, the guesses required to create populations of simulated spectra would become more and more questionable. For practical purposes, the last two rows of Table II provides an effective *minimal* estimate of retrieval errors from JIRAM data with the current code.

	$Log_{10}([H_2O]_{deep})$	$Log_{10}([H_2O]_{RH})$	$Log_{10}([NH_3]_{deep})$	$Log_{10}([PH_3]_{deep})$	$Log_{10}(\tau$ @ 5μ)
A priori					
$\sigma(x_a)$	1.0	0.48	0.56	0.63	1.
$\sigma(x)$	0.884	0.012	0.012	0.006	0.005
$<\Delta>_{ideal}$	0.048	-0.034	-0.006	-0.001	-0.007
$\sigma(\Delta)_{ideal}$	0.472	0.012	0.019	0.010	0.069
$<\Delta>_{irta}$	0.122	0.007	0.065	-0.002	-0.006
$\sigma(\Delta)_{irta}$	0.559	0.028	0.102	0.029	0.179

Table II. Retrieval performances of the analysis code, as inferred from numerical tests. $\sigma(x_a)$ elements are the corresponding standard deviations used to build the S_a covariance matrix. $\sigma(x)$ are the square roots of the solution covariance matrix S, as computed at the first iteration. $<\Delta>$ is the mean difference between true and retrieved value; $\sigma(\Delta)$ is the standard deviation of the difference between true and retrieved value. "ideal" subscript refers to the test on simulated observations computed using the same radiative transfer code embedded in the analysis code, "irta" (as for "inclusive of radiative transfer approximations") subscript refers to the test on simulated observations computed using a full line-by-line code inclusive of DISORT. The last two rows represents our best estimate of retrieval errors from the current code.

5. Use on real JIRAM data

The arrival of the Juno spacecraft at Jupiter allowed the first assessment of the actual instrument performances, namely:

- Observations of the sky away from Jupiter disk allow to estimate the component of the random error not associated to photon noise in the actual operative thermal conditions. This value turns out to vary between 1.5 and 5 $x10^{-2}$ μW/(cm^2 sr μm). On the other hand, photon noise inside the 5 μm transparency window has a similar magnitude: i.e.: maximum of $2x10^{-2}$ μW/(cm^2 sr μm). The quadratic sum of these figures provides a rough estimate of the effective NER of JIRAM spectra and demonstrates that over bright hot spots a signal-to-noise ratio exceeding 500 is commonly achieved.
- Spectra of IR bright regions allow to validate the spectral calibration. In the 5 μm transparency window the spectral sampling positions are essentially confirmed, while the effective spectral resolution is degraded by a factor of 1.3. Therefore, in this region the effective spectral resolution is about 16 nm.

Some further considerations arose from the retrieval code itself:

- It was immediately evident that germane and arsine must be included in the atmospheric composition, in order to properly match the spectra.

- An attempt was made to introduce a deep (5 bar) cloud, following the approach presented by [24], but this methodology demonstrated to produce negligible improvements of the fit quality in the analysis of JIRAM Hot Spots spectra and therefore represented, in our opinion, an unnecessary complication. This option can still be included for the analysis of other regions, since [25] suggested that a similar structure may exists at latitudes different than those typical of the Hot Spot occurrence.

Figure 8 shows two examples of retrievals using spectra extracted from the Hot Spot region of Fig. 1. In both cases, the average difference between observed and best fit spectrum are below 5%. Values of the atmospheric parameters retrieved in this region are discussed extensively in [26] and are essentially in line with previous expectations for Hot Spot conditions. Once the entire population of the spectral fit residuals from these observations is considered, some systematic differences (figure 9) can be noted:

- The depth of the strong minimum at 4.95-4.96 μm is seldom reproduced in the simulated spectra. This feature is associated to the water vapour absorption and cannot be improved including in the forward model the MT_CKD continuum [27]. Albeit similar models for water vapour continuum were used in past analyses of the Jupiter atmosphere [3], their use remains questionable, since they have been empirically derived for Earth-like conditions and their extension to the Jupiter H_2-dominated environment can produce systematic errors.
- A similar behaviour is observed for the minimum at 4.78 μm, associated to water vapour too.
- The weak minimum observed at 4.61 μm cannot be reproduced by our best fit spectra, as well as the flex at 4.57 μm. In our forward model we considered a spectral resolution degradation factor equal to 1.3, constant over the entire spectral range. This value however is purely empirical, and one may suppose that a lesser degradation around 4.6 μm could partially mitigate these misfits. This hypothesis however is not supported by tests with different degradation factors, where no clear trend in the quality of the fit can be derived in this spectral range.
- The peak at 4.69 μm appears often smoother in the best-fit spectra than in the observed ones.

Noteworthy, the misfits observed while modelling real JIRAM data show magnitudes similar to those described in fig. 3 and related to the forward model approximations. In particular, the region at 4.96 μm was one where the systematic and random components of the forward model errors is maximum. It is therefore reasonable to suspect that misfits presented in figure 9 are – at least partially – related to forward modelling approximations.

In these circumstances, the use of χ^2 to quantify fit quality results too punitive (unless the forward model error is considered to compute an "effective" NER) and we opted to consider in future science analysis the relative percentage discrepancy between observed and best-fit spectrum (averaged over the 4.6-5 μm range) as the most pertinent fit-quality parameter.

6. Future work

The development of the analysis code presented here had as a major goal to provide the JIRAM team a robust tool ready for the preliminary analysis of the data at the time of the first Juno pericenter passage. Going forward, there are a number of potential improvements we plan to test in the future:

1. *Set of retrieved parameters* In [2], we demonstrated that - even with the NER levels expected at that times (about 100 times higher than actually observed) – JIRAM spectra have about 17 degrees of freedom for signal, a number much higher than the number of variables currently retrieved. On the basis of the kernels curves presented in Figure 3 of [2], one can envisage as possible improvement the retrieval of the vertical profiles of water vapour (between 4 and 6.8 bars) and ammonia (between 4 and 6 bars), as well as the vertical profile of phosphine (in the rather large range between 1 and 6.8 bars).

2. *Forward methods* Tests on simulated observations demonstrated that the approximations in the forward model represent the main error source in our current analysis scheme. Among the improvements that can be made we can mention the replacement of the two-streams with the multiple-scattering matrix operator [28], also adopted in the well-established NEMESIS code [13]. More difficult is to envisage the complete replacement of the correlated-k approach: a full line-by-line treatment added to the scattering evaluation at each point of the pseudo-monochromatic grid is computationally too expensive. A possible alternative, is represented by the so-called 'correlated-I' method discussed in [29], but remains be tested under Jovian conditions.

Acknowledgements

This work was supported by the Italian Space Agency through ASI-INAF contract I/010/10/0 and 2014-050-R.0. JIL and SKA acknowledge support from NASA through the Juno Project. GSO acknowledges support from NASA through funds that were distributed to the Jet Propulsion Laboratory, California Institute of Technology.

H. Tran (Laboratoire Interuniversitaire des Systèmes Atmosphériques) kindly provided the code for line mixing of methane.

Development of the retrieval code greatly benefited of discussions with P. Irwin, L. Fletcher, R. Giles, T. Fouchet, P. Drossart, M. Roos-Serote and L. Kedziora-Chudczer

The JIRAM instrument has been developed by Leonardo at the Officine Galileo - Campi Bisenzio site.

The JIRAM instrument was conceived and brought to reality by our late collaborator and Institute director Dr. Angioletta Coradini (1946-2011).

References

[1] Adriani, A. et al. (2014) *JIRAM, the Jovian Infrared Auroral Mapper* Space Sci Rev, doi:10.1007/s11214-014-0094-y

[2] Grassi, D. et al. (2010) *Jupiter's hot spots: Quantitative assessment of the retrieval capabilities of future IR spectro-imagers*, Planetary and Space Science, 58, 1265-1278, doi:10.1016/j.pss.2010.05.003.

[3] Irwin, P. G. J., et al. (1998), *Cloud structure and atmospheric composition of Jupiter retrieved from Galileo near-infrared mapping spectrometer real-time spectra,* J. Geophys. Res., 103(E10), 23001–23021, doi:10.1029/98JE00948.

[4] Rodgers, C.R. (2000) *Inverse Methods for Atmospheric Sounding: Theory and Practice*, World Scientific, Singapore

[5] Adriani, A., et al. (2016) *Juno's Earth flyby: the Jovian infrared Auroral Mapper preliminary results*. Astrophysics and Space Science, 361 (8), article id.272.

[6] Fletcher, L. N. et al. (2016) *Mid-infrared mapping of Jupiter's temperatures, aerosol opacity and chemical distributions with IRTF/TEXES*, Icarus, 278, 128-161, doi:10.1016/j.icarus.2016.06.008.

[7] Atreya, S. K. et al. (1997) *Chemistry and Clouds of Jupiter's Atmosphere: A Galileo Perspective* in *The Three Galileos: The Man, the Spacecraft, the Telescope,* 249-260*,* doi:10.1007/978-94-015-8790-7_21

[8] Atreya, S. K., et al. (1999) *Comparison of the atmospheres of Jupiter and Saturn: deep atmospheric composition, cloud structure, vertical mixing, and origin*. Planet. Space Sci., 47, 1243-62. doi:10.1016/S0032-0633(99)00047-1.

[9] Drossart, P., et al. (1998), *The solar reflected component in Jupiter's 5-μm spectra from NIMS/Galileo observations*, J. Geophys. Res., 103(E10), 23043–23049, doi:10.1029/98JE01899

[10] Irwin, P. G. J., et al. (2001), *The Origin of Belt/Zone Contrasts in the Atmosphere of Jupiter and Their Correlation with 5-μm* Opacity, Icarus, 149, 397-415, doi:10.1006/icar.2000.6542.

[11] Sindoni, G., et al. (2017), *Characterization of the white ovals on Jupiter's southern hemisphere using the first data by the Juno/JIRAM instrument*, Geophys. Res. Lett., 44, doi:10.1002/2017GL072940.

[12] Grassi, D. et al. (2014) *The Venus nighttime atmosphere as observed by the VIRTIS-M instrument. Average fields from the complete infrared data set*, J. Geophys. Res. Planets, 119, 837–849, doi:10.1002/2013JE004586.

[13] Irwin, P. G. J., et al. (2007), *The NEMESIS planetary atmosphere radiative transfer and retrieval tool,* Journal of Quantitative Spectroscopy and Radiative Transfer, 109, 1136-1150, doi:10.1016/j.jqsrt.2007.11.006

[14] Kylling, A., et al. (1995) *A reliable and efficient two-stream algorithm for spherical radiative transfer: Documentation of accuracy in realistic layered media*, J. Atmos. Chem., 21, 115-150, doi:10.1007/BF00696577

[15] Seiff, A. et al. (1998) *Thermal structure of Jupiter's atmosphere near the edge of a 5-μm hot spot in the north equatorial belt*, J. Geophys. Res., 103(E10), 22857–22889, doi:10.1029/98JE01766. Available as numerical data as *GP-J-ASI-3-ENTRY-V1.0*, NASA Planetary Data System.

[16] Rothman, L.S., et al., (2013), *The HITRAN2012 molecular spectroscopic database*, J. Quant. Spectrosc. Radiat., 130, 4-50, doi: 10.1016/j.jqsrt.2013.07.002

[17] Tran, H., et al (2006) *Model, software, and database for line-mixing effects in the v_3 and v_4 bands of CH_4 and tests using laboratory and planetary measurements. H_2 (and He) broadening and the atmospheres of Jupiter and Saturn*, J. Quant. Spectrosc. Radiat. Tranf., 101**,** 306-324, doi:10.1016/j.jqsrt.2005.11.020

[18] Malathy Devi, V. et al., (2014a) *Line positions and intensities of the phosphine (PH_3) Pentad near 4.5 μm*, J. Mol. Spect. 289, 11-23, doi: 10.1016/j.jms.2014.01.013

[19] Malathy Devi, V. et al., (2014b) *Line shape parameters of PH_3 transitions in the Pentad near 4–5 μm: Self-broadened widths, shifts, line mixing and speed dependence*, J. Mol. Spect. 302, 17-33, doi: 10.1016/j.jms.2014.06.003

[20] Giles, R.S.., et al. (2015) *Cloud structure and composition of Jupiter's troposphere from 5-m Cassini VIMS spectroscopy*, Icarus, 257, 457-470, doi:10.1016/j.icarus.2015.05.030.

[21] Ragent, B., et al. (1998) *The clouds of Jupiter: Results of the Galileo Jupiter Mission Probe Nephelometer Experiment,* J. Geophys. Res., 103(E10), 22891–22909, doi:10.1029/98JE00353

[22] Press, W.H., et al., (1996) *Numerical Recipes in Fortran 90: The Art of Parallel Scientific Computing,* Cambridge University Press

[23] Stamnes, K., et al. (1998), *Numerically stable algorithm for discrete-ordinate-method radiative transfer in multiple scattering and emitting layered media*, Appl. Opt., 27 (12), 2502–2509

[24] Nixon, C.A. (2001) *Atmospheric Composition and Cloud Structure in Jovian 5-μm Hotspots from Analysis of Galileo NIMS Measurements*, Icarus, 150, 48-68, doi:10.1006/icar.2000.6561.

[25] Giles, R.S.., et al. (2016) *Latitudinal variability in Jupiter's tropospheric disequilibrium species: GeH_4, AsH_3 and PH_3*, accepted for publication in Icarus, arXiv:1610.09073

[26] Grassi, D. et al., (2017) *Preliminary results on the composition of Jupiter's troposphere in Hot Spots regions from the JIRAM/Juno instrument*, Geophys. Res. Lett., 44, doi:10.1002/2017GL072841

[27] Mlawer, E. J., et al. (2012) *Development and recent evaluation of the MT_CKD model of continuum absorption* Philos. Trans. Roy. Soc. London Ser. A, 370, 2520-2556, doi:10.1098/rsta.2011.0295.

[28] Plass, G.N., G.W. Kattawar, F.E. Catchings (1973) *Matrix operator theory of radiative transfer. 1: Rayleigh scattering*, Appl Opt, 12 , pp. 314–329

[29] Ignatiev, N.I., D. Grassi, L.V. Zasova (2005) *Planetary Fourier Spectrometer data analysis: Fast radiative transfer models*, Planetary and Space Sciences, Vol. 53, Issue 10, doi: 10.1016/j.pss.2004.12.009

425 Figures

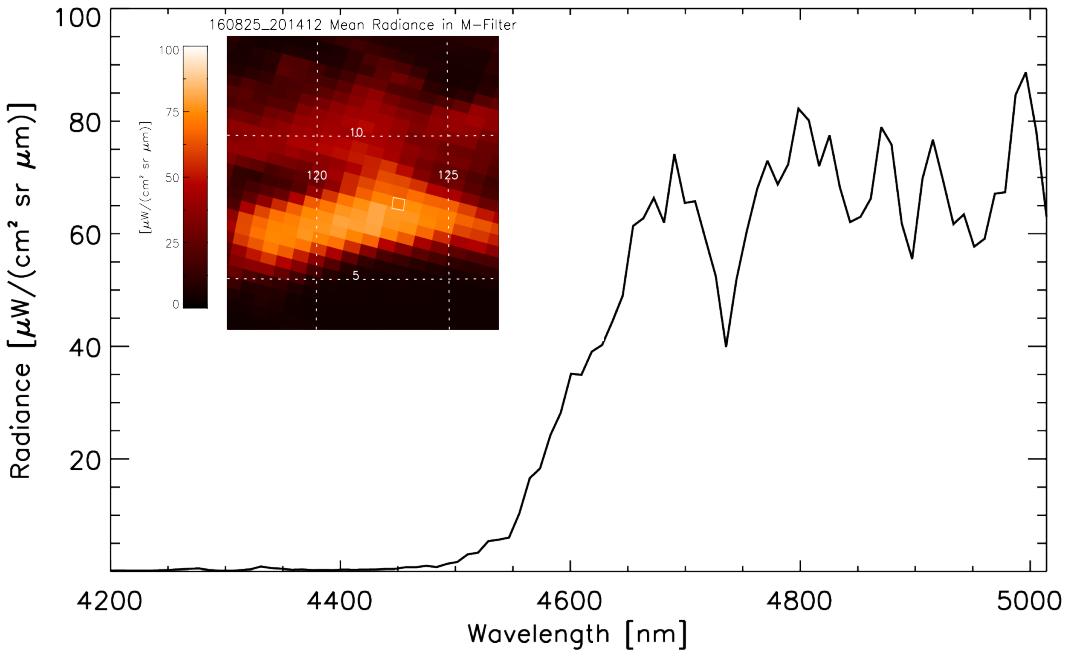

Fig. 1. Example of a JIRAM spectrum acquired in the brightest parts of a Jupiter Hot Spot (198th spectrum from frame JIR_SPE_RDR_2016238T205131_V01.DAT). The inset box map shows the spectrometer pixel borders. Spatial resolution is approximatively 500 km and emission angle is 29.5°.

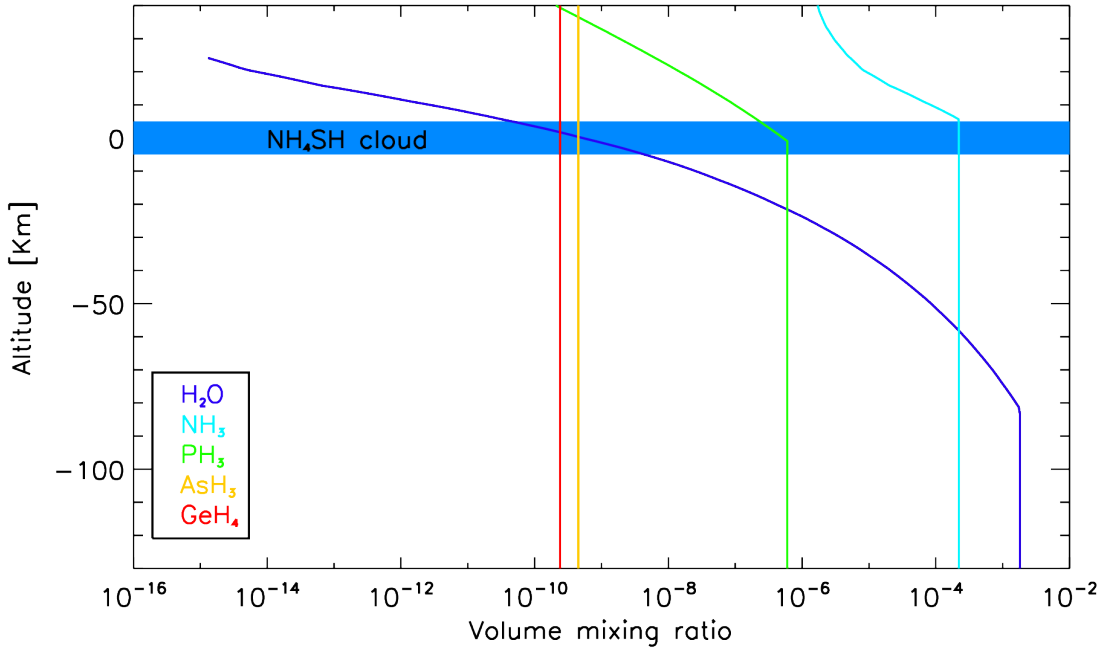

Fig. 2. Simplified gaseous mixing ratio profiles assumed as free parameters to fit observed spectra.

430

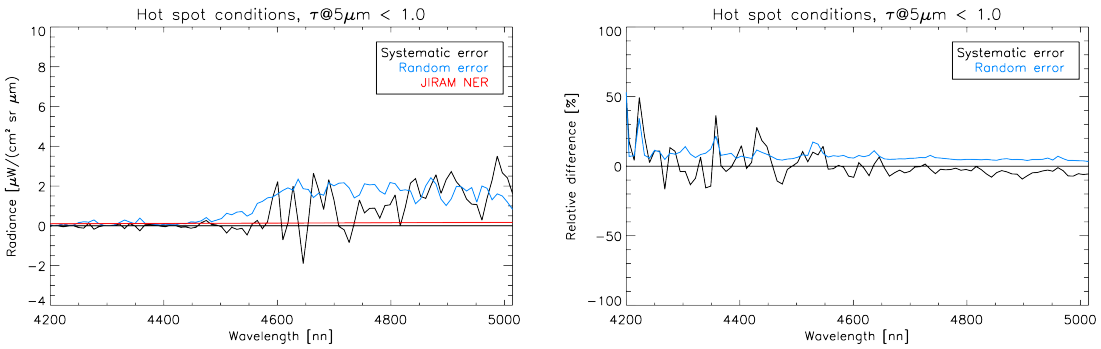

Fig. 3. Performances of the forward radiative transfer model embedded in the retrieval code, as assessed against the results obtained using a full line-by-line code based on DISORT and with a high density vertical sampling. Panel a.: systematic and random components of differences, in absolute terms. Panel b.: systematic and random components of differences, in relative terms with respect to line-by-line code.

435

440

445

450

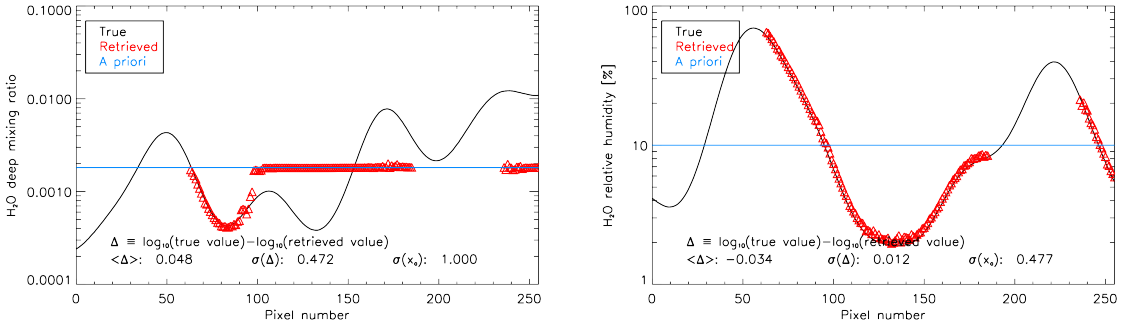

a b

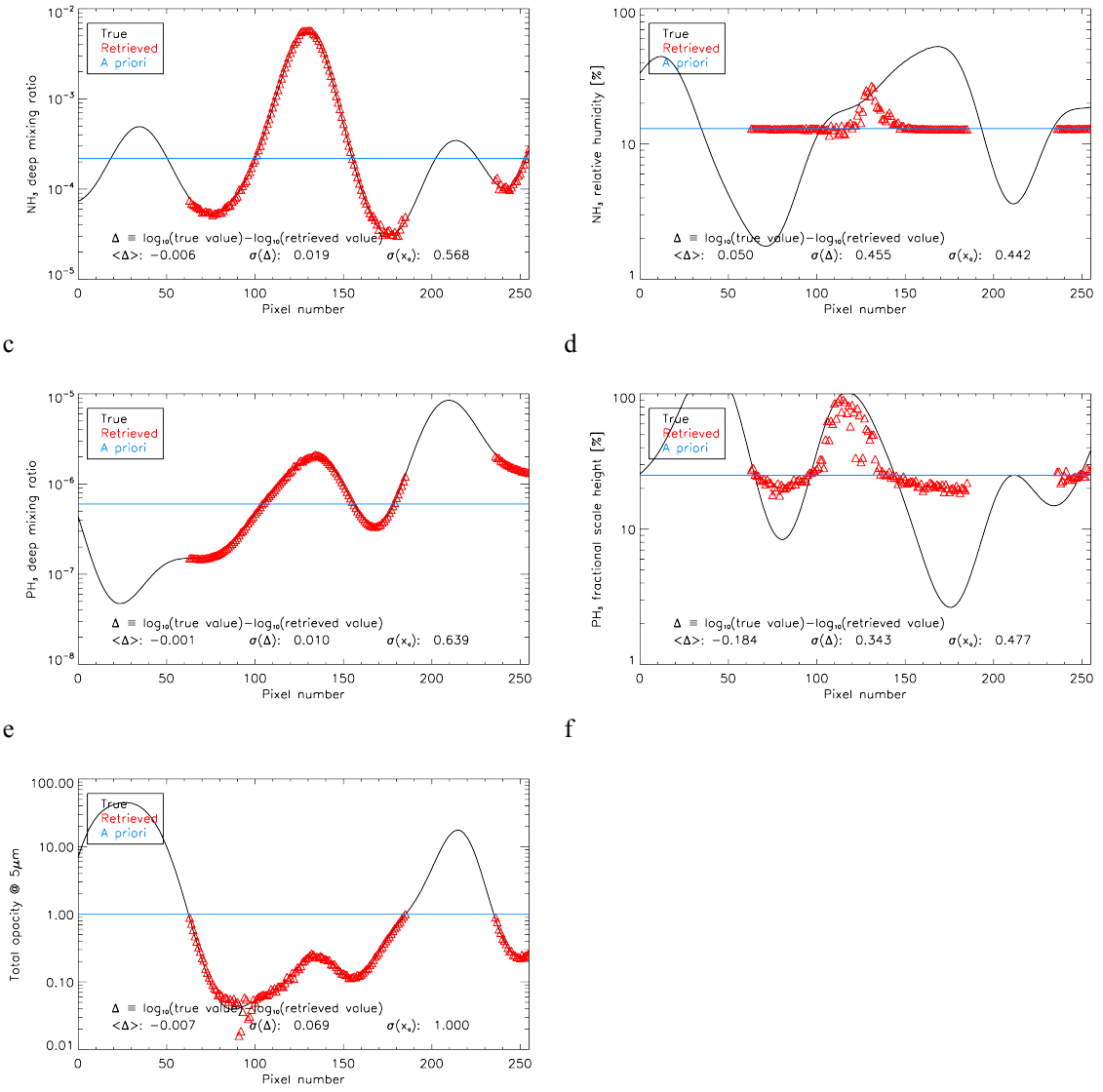

Fig. 4. Retrieval performances of analysis code, as estimated from a test run on a population of simulated observations. Each panel compares the input values (black curves) used to compute the simulated spectra against the retrieved values (red triangles). Each triangle corresponds to an individual spectrum, independently analysed. Comparison is performed only for cases where residual opacity of 1-bar cloud is less than 1. Each panel reports also: $<\Delta>$, the mean difference between true and retrieved value; $\sigma(\Delta)$, the standard deviation of the difference between true and retrieved value; $\sigma(x_a)$, the standard deviation of the corresponding element in the a priori state vector. Panel a: $\log_{10}$ of deep water vapour mixing ratio; Panel b: $\log_{10}$ of water vapour relative humidity; Panel c: $\log_{10}$ of deep ammonia mixing ratio; Panel d: $\log_{10}$ of ammonia relative humidity; Panel e: $\log_{10}$ of deep ammonia mixing ratio; Panel f: $\log_{10}$ of phosphine relative scale height; Panel g: $\log_{10}$ of 5 μm opacity of the residual 1-bar cloud

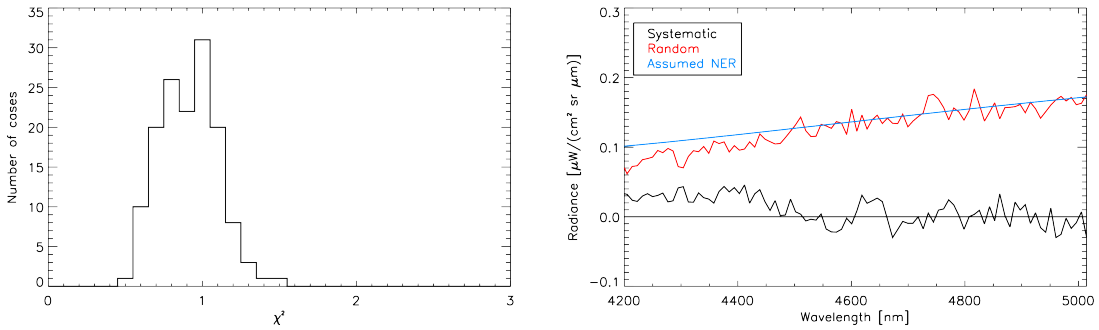

a b

Fig. 5. Modelling performances of analysis code, as estimated from a test run on a population of simulated observations. For both panels, only cases where residual opacity of 1-bar cloud is less than 1 were considered. Panel a: distribution of χ^2 for fit residuals. Panel b: differences between observed (simulated) data and best-fit spectra. Black curve ("systematic"): mean difference, as computed over the population; red curve ("random"): standard deviation of the difference; blue curve: NER value assumed for the test.

455

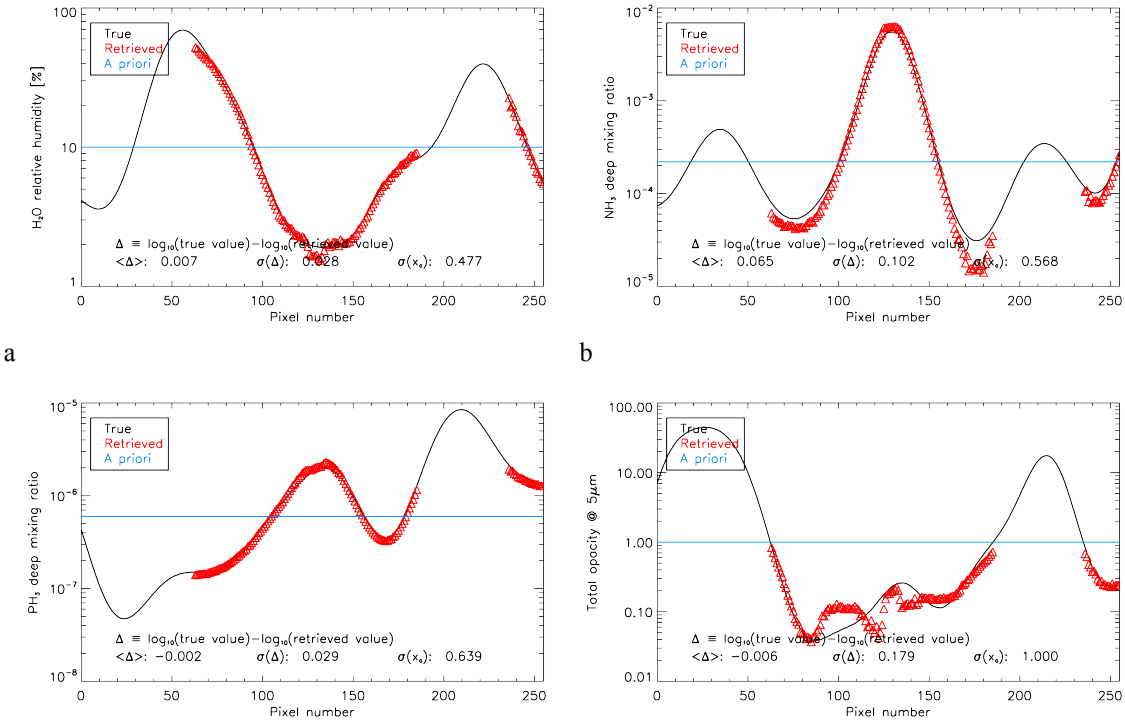

Fig. 6. The same as fig. 4, but applying the analysis code to a population of simulated spectra computed using a full line-by-line code inclusive of DISORT. This test provides our current best simulation of actual operative conditions.

460

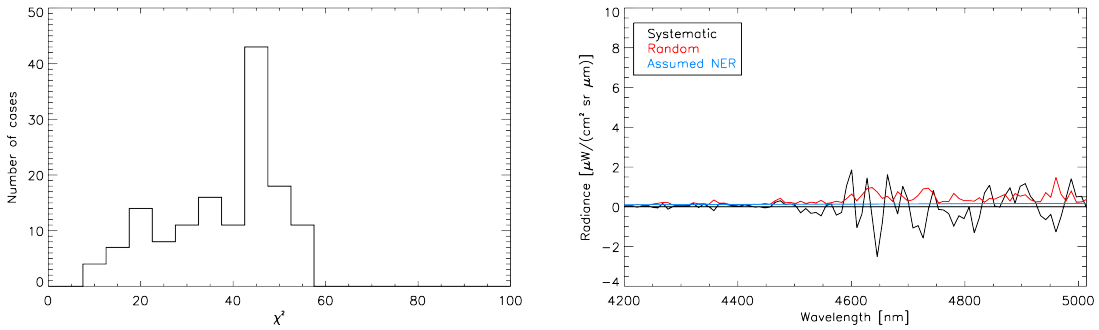

a b

Fig. 7. The same of fig. 5, but applying the analysis code to a population of simulated spectra computed using a full line-by-line code inclusive of DISORT.

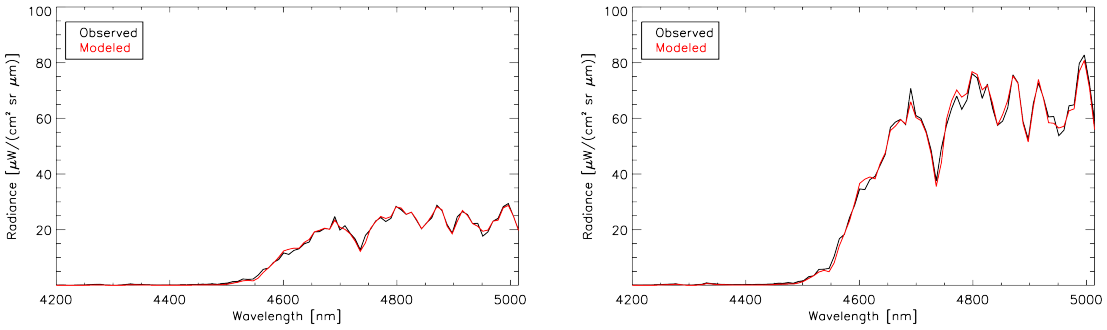

a b

Fig. 8. Two examples of fitting of actual JIRAM data. Both examples are from the same Hot Spot presented in fig. 1 and extensively discussed in [27].

465

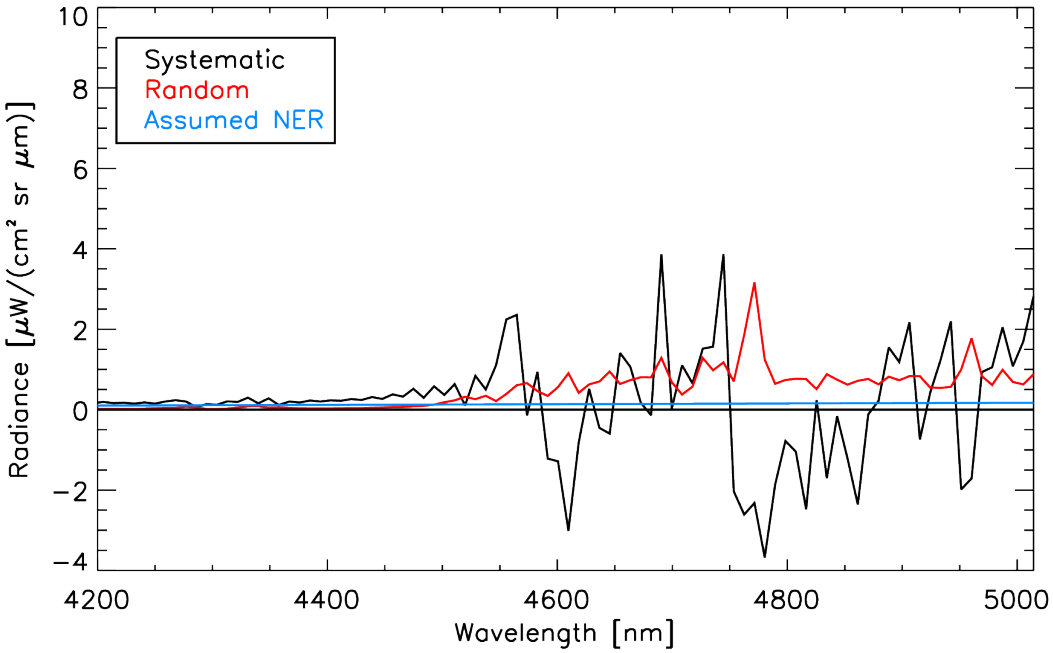

Fig. 9. Modelling performances of analysis code once applied to actual JIRAM data, as estimated from the differences between observed data and best-fit spectra. Black curve ("systematic"): mean difference, as computed over the population; red curve ("random"): standard deviation of the difference; blue curve: NER value assumed for the test. Statistic were computed from spectra with a retrieved opacity < 1 from Hot Spot #1 discussed in [27], the same presented in fig.1.

470